Nucleomorph phylogenomics suggests a deep and ancient origin of cryptophyte plastids within Rhodophyta

Lukas V. F. Novak[1,2]*, Sergio A. Muñoz-Gómez[1,3], Fabian van Beveren[1,4], Maria Ciobanu[1], Laura Eme[1], Purificación López-García[1], David Moreira[1]*

1) Unité d'Ecologie Systématique et Evolution, CNRS, AgroParisTech, Université Paris-Saclay, Gif-sur-Yvette, France.

2) Biologie et Ecologie des Ecosystèmes Marins Profonds (BEEP), CNRS, Université de Bretagne Occidentale, Institut Universitaire Européen de la Mer, Plouzané, France.

3) Department of Biological Sciences, Purdue University, IN, USA.

4) Laboratoire de Recherche en Sciences Végétales (LRSV), Université de Toulouse, CNRS, Castanet Tolosan, France.

* lukas.novak@univ-brest.fr (LVFN), david.moreira@universite-paris-saclay.fr (DM)

Abstract

The evolutionary origin of red algae-derived complex plastids remains obscure. Cryptophyta, one of four eukaryotic lineages harboring these plastids, still contain nucleomorphs, highly reduced remnants of red algal nuclei. The genes present on nucleomorph genomes can be used for phylogenomic reconstruction in order to unravel the evolutionary origin of all red complex plastids and provide data independent from previously analyzed plastid-encoded datasets. Here, we leverage these genes in a first attempt at pinpointing the position of cryptophyte nucleomorphs within a comprehensive diversity of Rhodophyta, including new sequence representatives from seven deep-branching red algae. Our analyses place cryptophyte nucleomorphs as sister to the extremophilic subphylum Cyanidiophytina. This conflicts with published analyses based on plastidial genes that placed red complex plastids closer to the mesophilic Rhodophytina. Our results reject a nucleomorph origin within any known subgroup of Rhodophyta, instead suggesting a deep and possibly freshwater origin of complex red plastids.

Introduction

The origin of complex plastids of red algal (Rhodophyta) ancestry found in photosynthetic members of Cryptista, Alveolata, Stramenopiles, and Haptista ("CASH") remains one of the great unresolved questions of eukaryotic evolution. Two competing hypotheses have tried to explain the presence of these organelles of apparently shared origin in these four not-so-closely-related lineages of hosts (Yoon et al. 2002; Burki et al. 2020). On the one hand, the chromalveolate hypothesis (Cavalier-Smith 1999) posits a single origin of these plastids from a single secondary endosymbiosis event in a common ancestor of CASH, and its subsequent vertical inheritance accompanied by multiple independent plastid losses in non-photosynthetic CASH species. On the other hand, the serial endosymbiosis hypothesis (Sanchez-Puerta and Delwiche 2008) postulates that secondary endosymbiosis occurred more recently in a single CASH lineage, after the four lineages had already diverged, and spread to the rest horizontally *via* tertiary, or even higher-degree, endosymbioses. This serial endosymbiosis hypothesis has been proposed in multiple versions positing different numbers and order of symbiotic events (Sanchez-Puerta and Delwiche 2008; Petersen et al. 2014; Stiller et al. 2014; Bodył 2018).

Regardless of which particular scenario is true, the identity of the red algal donor of complex plastids requires further investigation. Phylogenomic analyses of plastid-encoded genes (Yoon et al. 2002; Iida et al. 2007; Janouškovec et al. 2010; Stiller et al. 2014; Ševčíková et al. 2015; Kim et al. 2017) have consistently placed the CASH complex plastids in the vicinity of the Rhodophytina, the mesophilic branch of Rhodophyta, as opposed to the ancestrally extremophilic, freshwater Cyanidiophytina (Yoon et al. 2017). However, our insufficient understanding of phylogenetic relationships between red algal groups, as well as poor taxon sampling of rhodophyte genomes, have for a long time limited the usefulness of such studies in precisely pinpointing the donor taxon. Recent large-scale phylogenomic analyses of plastid-

51 and mitochondrion-encoded genes (Muñoz-Gómez et al. 2017; van Beveren et al. 2022) have
52 greatly advanced our understanding of the internal phylogeny of the phylum Rhodophyta.
53 These analyses support the basic division between Cyanidiophytina (class Cyanidiophyceae)
54 and Rhodophytina and split the latter into two monophyletic subphyla: Proteorhodophytina
55 (classes Compsopogonophyceae, Porphyridiophyceae, Rhodellophyceae, and
56 Stylonematophyceae), comprising red algae with single-celled or simple multicellular body
57 plans, and Eurhodophytina (classes Bangiophyceae and Florideophyceae), with complex
58 multicellularity.

59 To attempt to phylogenetically place CASH plastids within the tree of Rhodophyta, we used
60 an alternative source of genetic data – the nucleomorph genomes of Cryptophyta (Cryptista).
61 Nucleomorphs (NMs) are highly reduced nuclei of archaeplastid algae that reside in the
62 periplastidial space of certain complex plastids. There are at least three independent examples
63 of NMs derived from green algae (Ludwig and Gibbs 1989; Sarai et al. 2020), but only one
64 derived from red algae (Ludwig and Gibbs 1987; Douglas et al. 2001). These organelles are
65 relatively well studied; phylogenetic analyses of their rRNAs have suggested a rhodophyte
66 origin (Douglas et al. 1991; Maier et al. 1991), and they have even been included in exploration
67 of rhodophyte genomic diversity (Wong et al. 2023). However, to our knowledge, there has
68 not been any published phylogenomic analysis attempting to locate the position of cryptophyte
69 NMs within Rhodophyta. Cryptophyte NMs contain several hundred open reading frames
70 (ORFs) that can be divided into three categories: conserved ORFs with annotated homologues
71 outside cryptophyte NMs, "nORFs" with annotated homologues only in other cryptophyte
72 NMs, and "ORFans" without recognizable sequence similarity to any other known sequence
73 (Moore et al. 2012). Only conserved ORFs are therefore useful for phylogenomic analyses
74 aiming at placing NMs in a broader eukaryotic context. With this goal in mind, we have
75 improved the taxon sampling of red algae by sequencing seven novel nuclear genomes and

performed a series of phylogenomic investigations into the position of cryptophyte NMs among Rhodophyta using a large dataset of 180 conserved ORFs.

Results and Discussion

To improve the taxon sampling of nucleus-encoded protein sequences of Rhodophyta available for phylogenomic analyses, we sequenced DNA of seven red algae: *Galdieria* sp. ACUF 613 (Cyanidiophyceae), *Madagascaria erythrocladioides* (Compsopogonophyceae), *Erythrolobus coxiae*, *Porphyridium aerugineum*, *Timspurckia oligopyrenoides* (Porphyridiophyceae), *Dixoniella grisea*, and *Rhodella violacea* (Rhodellophyceae). We assembled their nuclear genomes and predicted protein-coding genes. These new sequences, together with previously published genome- and transcriptome-derived predicted proteomes available in the EukProt database (Richter et al. 2022), cover all seven classes of Rhodophyta and, for the first time, allow analyzing the cryptophyte NMs phylogenetic position in relation to the full known diversity of red algae.

In order to maximize the independence of our phylogenomic matrix from plastid data, we started with a seed dataset of 230 NM-encoded proteins (markers) from the non-photosynthetic cryptophyte *Cryptomonas paramecium*, which were annotated as not being associated with the plastid (Tanifuji et al. 2010). Our final phylogenomic sequence supermatrix contained 51,610 amino acid positions belonging to 180 housekeeping protein markers (annotation in supplementary file S1); it included 54 species covering Viridiplantae, Glaucophyta, *Rhodelphis*, all seven classes of Rhodophyta including three of the four known orders of Cyanidiophyceae (Park et al. 2023), and NMs of four distantly related cryptophyte species:

97 *C. paramecium*, *Guillardia theta*, *Chroomonas mesostigmatica*, and *Hemiselmis andersenii*
98 (Hoef-Emden et al. 2002; Kim and Archibald 2013; Greenwold et al. 2023).

99 We carried out phylogenomic analyses of the sequence matrix by maximum likelihood (ML)
100 with the LG+C60+G+F mixture model and by Bayesian inference with the CAT-GTR model.
101 The resulting trees were outgroup-rooted on the non-rhodophyte archaeplastida. Both analyses
102 (figure 1) recovered the expected topology of Archaeplastida and Rhodophyta, including the
103 monophyly of Proteorhodophytina with full support (1/100/100: Bayesian posterior
104 probability/ultrafast bootstrap/nonparametric bootstrap). Surprisingly, the analyses recovered
105 the cryptophyte NMs as sister to Cyanidiophytina with strong support (1/99/99). This result is
106 conflicting with all previously published phylogenomic analyses of CASH plastids (including
107 Cryptophyta) based on plastid-encoded genes, which unanimously placed CASH as sister to
108 the other major branch of red algae, the Rhodophytina. To test the robustness of the recovered
109 topology, we carried out a series of analyses (tests 1–8) designed to uncover potential influence
110 of long-branch or compositional attractions on the ML results (figure 2).

111 We first inferred individual phylogenetic trees for each of the 180 markers, and then
112 progressively removed from the supermatrix the markers producing the longest trees based on
113 (1) the length of the NM stem branch (first common ancestor to last common ancestor of NMs;
114 test 1), and (2) the average length of the NM branches, from the last common ancestor of NMs
115 to the tips (test 2). We also progressively removed individual long-branching NM sequences
116 based on their cumulative branch length from the root of NMs to the tip (test 3). For test 4, we
117 used the estimated evolutionary rate of each position in the supermatrix to progressively
118 remove the fastest-evolving sites. For test 5, we evaluated the amino acid composition of
119 sequences from individual species in the supermatrix; we determined that cryptophyte NMs
120 are significantly enriched in F, S, I, N, and K and depleted in A, P, V, D, and M amino acids,

121 while Cyanidiophytina orthologs are moderately enriched in L and W amino acids (figure 2F).
122 We thus progressively removed the most compositionally biased sites in the NMs from the
123 supermatrix.

124 For all these tests, we inferred ML trees from supermatrices generated by gradually reducing
125 divergent data in increments of 10%. Subsequently, we visualized the fluctuations in ultrafast
126 bootstrap statistical support for the branches of interest. (figure 2A–E). Only in test 2 do we
127 see the support for the monophyly of cryptophyte NMs and Cyanidiophytina substantially drop,
128 and an alternative topology (NMs sister to all Rhodophyta) rose over 50% support in a single
129 tree (with 60% of markers remaining). None of the other tests showed this alternative topology
130 and the support for NMs sister to Cyanidiophytina remained above 90%.

131 For test 6, we recoded the supermatrix into a four-character state amino acid alphabet in order
132 to minimize phylogenetic artefacts stemming from poorly modelled compositional
133 heterogeneity (Susko and Roger 2007; Brown et al. 2013). The resulting ML tree presented the
134 same topology as the original with 99% support for NMs as sister to Cyanidiophytina (figure
135 2G).

136 In test 7, we performed the Approximately Unbiased (AU) test (Shimodaira 2002) to compare
137 the original tree with alternative topologies (figure 2H). The AU test rejected all topologies
138 except for the original ML tree (figure 2G: topology 7.1); the topology consistent with the
139 previous plastid-encoded proteins analyses i.e., NMs sister to Rhodophytina could not be
140 rejected, although the p-value (0.0924) was on the cusp of the cut-off for significance (figure
141 2G: topology 7.3). Notably, the topology briefly supported in test 2 (figure 2G: topology 7.2)
142 was rejected by the AU test (p-value=0.0154).

143 Finally, in test 8, we removed 7% of the most functionally divergent sites from the supermatrix,
144 as estimated by FunDi (Gaston et al. 2011), in order to evaluate the effect of functional

145 divergence in the protein sequences. This aimed to reduce potential artefacts from model
146 misspecification since phylogenetic model currently available do not properly capture
147 functional divergence in proteins (Inagaki et al. 2003; Muñoz-Gómez et al. 2022). ML
148 phylogenetic analysis of the resulting supermatrix again recovered the original topology with
149 99% support for the monophyly of NMs and Cyanidiophytina (figure 2G).

150 Taken together, our analyses show that the hypothesis of cryptophyte NMs branching sister to
151 Cyanidiophytina is the one best supported by housekeeping genes still preserved in cryptophyte
152 nucleomorph genomes. There is no indication whatsoever that this result was influenced by
153 long-branch attraction or compositional bias. However, the previously suggested position of
154 NMs as sister to Rhodophytina is not strongly rejected by the NM data and given its recovery
155 in plastid genome phylogenetic analyses (Iida et al. 2007; Janouškovec et al. 2010; Ševčíková
156 et al. 2015; Kim et al. 2017), we cannot at this stage favor one over the other.

157 Most importantly, our analyses neither show a close relationship between cryptophyte NMs
158 and any of the six classes of Rhodophytina, nor their origin from within the known extant
159 diversity of Cyanidiophytina. On the contrary, they support a deep and ancient origin of the
160 cryptophyte NMs and, therefore, presumably also of all CASH plastids, within red algae. They
161 likely emerged as sister to either Cyanidiophytina or Rhodophytina, two alternative positions
162 placed just a single node away from each other.

163 Our results suggest that the secondary red endosymbiosis occurred either before the
164 diversification of extant rhodophyte classes, or later, from a so-far-unknown deep branching
165 lineage of red algae. This currently unknown lineage has either gone extinct (except for the
166 complex plastids derived from it) or still exists, waiting to be discovered. Indeed, the discovery
167 of a novel deep branching lineage in the phylogenetic vicinity of Rhodophyta would not be
168 unprecedented (Gawryluk et al. 2019) and, as recent advances in primary endosymbiosis

169 research indicate (Ponce-Toledo et al. 2017) , it may take a lucky find of a microbe closely
170 related to our organelle of interest to resolve a long-standing disagreement between
171 evolutionary scenarios. Furthermore, if the sister position of cryptophyte NMs to
172 Cyanidiophytina recovered in our analyses gets confirmed, it would support a freshwater and/or
173 thermoacidophilic ancestry of CASH plastids, consistent with the notion that most of the early
174 evolution of photosynthetic eukaryotes occurred in freshwater environments (Lewis 2017;
175 Ponce-Toledo et al. 2017; Sánchez-Baracaldo et al. 2017).

176 **Materials and Methods**

177 For culturing, DNA extraction, and sequencing methods see (van Beveren et al. 2022). Raw
178 genomic reads obtained by Illumina HiSeq 2500 and NovaSeq 6000 (for *D. grisea*, *E. coxiae*,
179 *Galdieria* sp. ACUF 613, *M. erythrocladioides*, *P. aerugineum*, and *T. oligopyrenoides*) and
180 by Illumina HiSeq 2500 and NovaSeq 6000 plus Oxford Nanopore MinION Mk 1B (for
181 *R. violacea*) were assembled using SPAdes assembler, version 3.14.1 (Prjibelski et al. 2020).
182 Nuclear contigs were separated from organellar and prokaryotic contamination-derived
183 sequences using Whokaryote, version 1.1.2 (Pronk and Medema 2022). Raw reads were
184 mapped to resulting contigs using the BWA-MEM algorithm (github.com/lh3/bwa) and
185 BLASTn (Altschul et al. 1990) was used to search the contigs against the NCBI nt database,
186 release 240. Results of the read mapping and BLASTn search were visualized in BlobTools2
187 (Challis et al. 2020) and used for additional manual decontamination, resulting in preliminary
188 genomic assemblies (not shown).

189 Previously published transcriptomic reads for *M. erythrocladioides* (SRX554333),
190 *T. oligopyrenoides* (SRX554192), and *R. violacea* (ERX2100208) were downloaded from the
191 NCBI SRA database and mapped to their respective genomic assemblies using the BWA-MEM
192 algorithm and visualized in the Integrative Genomics Viewer, version 2.9.4 (Robinson et al.

193 2011). Sets of >200 protein-coding gene models were manually predicted for each of the three
194 assemblies with mapped transcripts and used as training sets for the online AUGUSTUS gene
195 predictor (Hoff and Stanke 2013). The resulting species parameters, as well as previously
196 available *Galdieria sulphuraria* (Cyanidiophyceae) species parameters, were used in parallel
197 for AUGUSTUS automatic gene prediction based on each of the seven genomic assemblies.
198 The completeness of the individual sets of AUGUSTUS-predicted genes was evaluated using
199 BUSCO, version 5.4.3, with the eukaryota_odb10 dataset (Manni et al. 2021) and the one with
200 the highest estimated completeness was selected for each of the seven assemblies. These
201 preliminary predicted proteomes were searched for protein sequences of interest for use in
202 further analyses.

203 The 230 *C. paramecium* NM-encoded protein sequences from the "Conserved ORFs" dataset
204 (Tanifuji et al. 2010) were searched against a custom protein database consisting of the seven
205 novel rhodophyte preliminary predicted proteomes plus three cryptophyte NM predicted
206 proteomes downloaded from the NCBI GenBank database, release 245, and multiple predicted
207 proteomes representing a broad diversity of eukaryotes downloaded from the EukProt database,
208 version 2 (Richter et al. 2022). Two best (lowest E-value) BLASTp hits were recovered per
209 proteome for each query sequence. The sequences were aligned using MAFFT, version 7.455
210 (Katoh and Standley 2013) and resulting alignments were trimmed using BMGE, version 1.12
211 (Criscuolo and Gribaldo 2010) and then used to reconstruct initial single-gene trees using
212 FastTree, version 2.1.8 with JTT+CAT model (Price et al. 2010). The trees (supplementary file
213 S2) were manually inspected and used to: 1) select 180 proteins that produced trees where all
214 the NM sequences branched together to the exclusion of all other sequences, 2) select 54
215 proteomes most relevant to the studied question, i.e. four from cryptophyte NMs and 50 from
216 four lineages of Archaeplastida (Rhodophyta, *Rhodelphis*, Glaucophyta, and Viridiplantae),
217 and 3) when paralogs were present, select a single paralog per tree – determined by a shorter

218 branch. This selection resulted in the initial phylogenomic dataset of 180 markers in 54 species.
219 Details about the selected species are shown in supplementary file S3.

220 The selected protein sequences were gathered in full length into 180 single-gene multi-FASTA
221 files. PREQUAL, version 1.01 (Whelan et al. 2018) was used to identify and mask positions
222 with non-homologous characters and the masked sequences were aligned using MAFFT,
223 version 7.455 (Katoh and Standley 2013). The alignments were then trimmed using DIVVIER
224 (-partial -mincol 28), version 1.01 (Ali et al. 2019). The resulting alignments (supplementary
225 file S4) were used to reconstruct single-marker phylogenetic trees as well as to assemble a
226 concatenated supermatrix using phyutility, version 2.2 (Smith and Dunn 2008). Details about
227 the matrix are shown in supplementary file S1.

228 The supermatrix (supplementary file S5) was analyzed with IQ-TREE, version 2.2.0 (Minh et
229 al. 2020) using the substitution model LG+C60+G+F and both ultrafast bootstrap (-bb 1000)
230 and nonparametric bootstrap (-bo 100) for the maximum likelihood (ML) phylogenetic analysis
231 and with PhyloBayes-MPI, version 1.8c (Lartillot et al. 2013) with the CAT-GTR substitution
232 model (Lartillot and Philippe 2004) for the Bayesian inference phylogenetic analysis (figure
233 1). The PhyloBayes-MPI analysis with two chains was run for more than 50,000 generations.
234 The chains did not converge (maxdiff=1, meandiff=0.0190534, burn-in: 1000, sub-sampling
235 every 10 trees), as is often the case with large phylogenomic datasets. Trace files were
236 inspected with Tracer (Rambaut et al. 2018). Trees were visualized and edited using
237 TreeViewer, version 2.1.0 (Bianchini and Sánchez-Baracaldo 2024).

238 Single-marker trees (supplementary file S6) were reconstructed using IQ-TREE (-bb 1000 -m
239 LG+C60+G+F) version 2.2.0. PhyKIT, version 1.11.3 (Steenwyk et al. 2021) was used to
240 extract branch lengths in the 180 single-marker trees and this information guided further tests
241 of topology robustness by sequential removal of markers or individual sequences.

242 In test 1, all markers were sorted by the length of the root branch of cryptophyte NMs (first
243 common ancestor to last common ancestor of NMs) from longest to shortest to generate
244 additional supermatrices, by removing, in a stepwise fashion, 10% of the markers. In test 2, all
245 markers were sorted by the average compound length of cryptophyte NM branches (first
246 common ancestor of NMs to tips) from longest to shortest to generate 8 supermatrices, by
247 removing, in a stepwise fashion, 10% of the markers. In test 3, only individual sequences were
248 removed, not entire markers. All NM sequences were sorted by their compound branch length
249 (first common ancestor of NMs to tips) from longest to shortest to generate 8 supermatrices,
250 by removing, in a stepwise fashion, 10% of the NM sequences. In this test, 14 sequences (from
251 NMs, Rhodophyta, and *Rhodelphis*), identified in the IQ-TREE-generated single-marker trees
252 as disrupting NM monophyly, were removed together with the first 10% longest-branch
253 sequences. Details about the removed markers and sequences and their sorting in tests 1–3 are
254 shown in supplementary file S7.

255 In test 4, IQ-TREE, version 2.2.0 was used to calculate site-specific evolutionary rates (--rate
256 -mlrate -m LG+C60+G+F) for each position in the original supermatrix (supplementary file
257 S8) and SiteStripper, version 1.02 (github.com/hverbruggen/SiteStripper) was used to generate
258 8 supermatrices, each by removing, in a stepwise fashion, 10% of the positions with the highest
259 evolutionary rates.

260 In test 5, amino acid compositional bias of the species in the supermatrix was determined
261 according to the $\chi 2$ metric as described before (Viklund et al. 2012; Martijn et al. 2018; Muñoz-
262 Gómez et al. 2019). Occurrences of all amino acids in all positions in the matrix were counted
263 and the positions were sorted according to the ratio F+S+I+N+K / A+P+V+D+M in NMs
264 divided by the ratio F+S+I+N+K / A+P+V+D+M in all other species. In order to avoid dividing
265 by zero, an arbitrary value of 0.01 was added to all the amino acid occurrence values before

266 the calculation. Details about this calculation and sorting are given in supplementary file S9. A
267 custom Python script was used to generate 8 supermatrices, each with 10% of the remaining
268 positions removed starting with those with NMs most enriched in F+S+I+N+K and other
269 species most depleted in A+P+V+D+M.

270 The modified supermatrices generated in tests 1–5 were used to reconstruct ML trees (IQ-
271 TREE, -bb 1000 -m LG+C60+G+F) and the ultrafast bootstrap values supporting the original
272 or alternative positions of NMs within the resulting topologies were plotted in figure 2.

273 To further evaluate the effects of compositional heterogeneity on phylogenetic inference, in
274 test 6, we recoded the supermatrix into a four-character state amino acid alphabet that
275 minimizes the compositional heterogeneity present in the data. The program minmax-chisq,
276 which implements the methods of Susko and Roger (Susko and Roger 2007), was used to find
277 the best recoding scheme for our supermatrix. The best recoding scheme (S4) was found to be
278 NQFPV, RDCLKMST, AEGHIY, and W. Phylogenetic analyses on the recoded supermatrix
279 were performed with IQ-TREE, version 2.2.2.7 and the across-site compositionally
280 heterogeneous GTR+C60(S4)+F+R6 model. C60(S4) is an adaptation of the C60 mixture
281 model to four-character states. It is obtained by adding the frequencies of the amino acids that
282 belong to each bin in the dataset-specific four-character state scheme S4.

283 In test 7, we calculated ML trees (IQ-TREE, -bb 1000 -m LG+C60+G+F) with alternative
284 topologies by constraining possible relationships under following scenarios: 1) unconstrained
285 original tree, i.e. NMs+Cyanidiophytina, 2) NMs outside Rhodophyta, 3) NMs+Rhodophytina,
286 4) NMs+Eurhodophytina, and 5) NMs+Proteorhodophytina. AU-test (Shimodaira 2002) was
287 used as implemented in IQ-TREE (-m LG+C60+G+F -n 0 -zb 1000 -au) to test the alternative
288 hypotheses.

289 To evaluate the effect of functional divergence in the protein sequences, in test 8 we used the
290 software FunDi, version 1.1 (Gaston et al. 2011) to estimate functionally divergent sites in the
291 branch that separates nucleomorphs from all other nuclear genomes. About 7% of all amino
292 acid sites were estimated to be functionally divergent with a posterior probability of > 0.5.
293 These were subsequently removed using a custom Perl script. The resulting supermatrix
294 consisted of 47,951 amino acids. Phylogenetic analyses on the supermatrix without
295 functionally divergent sites were performed with IQ-TREE version 2.2.2.7 and the across-site
296 compositionally heterogeneous LG+C60+G4+F mixture model. All alternative trees used in
297 the tests can be found in supplementary file S10.

298 **Data Availability**

299 All new sequences used in the phylogenomic analysis were deposited in NCBI GenBank under
300 accession numbers PP113013–PP114032.

301 **Acknowledgments**

302 This work was funded by the European Research Council Advanced Grants Protist World
303 (No. 322669, P.L.-G.) and Plast-Evol (No. 787904, D.M.) and the ERC Starting grant
304 MacroEpik (No. 803151, L.E.). We thank the UNICELL single-cell genomics platform
305 (deemteam.fr/en/unicell) for help in DNA preparation and Nanopore sequencing.

306 **References**

307 Ali RH, Bogusz M, Whelan S. 2019. Identifying clusters of high confidence homologies in
308 multiple sequence alignments. *Molecular Biology and Evolution* 36:2340.

309 Altschul SF, Gish W, Miller W, Myers EW, Lipman DJ. 1990. Basic local alignment search
310 tool. *Journal of Molecular Biology* 215:403–410.

311 van Beveren F, Eme L, López-García P, Ciobanu M, Moreira D. 2022. Independent size
312 expansions and intron proliferation in red algal plastid and mitochondrial genomes.
313 *Genome Biology and Evolution* 14:evac037.

314 Bianchini G, Sánchez-Baracaldo P. 2024. TreeViewer: Flexible, modular software to
315 visualise and manipulate phylogenetic trees. *Ecology and Evolution* 14:e10873.

316 Bodył A. 2018. Did some red alga-derived plastids evolve via kleptoplastidy? A hypothesis.
317 *Biological Reviews* 93:201–222.

318 Brown MW, Sharpe SC, Silberman JD, Heiss AA, Lang BF, Simpson AGB, Roger AJ. 2013.
319 Phylogenomics demonstrates that breviate flagellates are related to opisthokonts and
320 apusomonads. *Proceedings of the Royal Society B: Biological Sciences*
321 280:20131755.

322 Burki F, Roger AJ, Brown MW, Simpson AGB. 2020. The new tree of Eukaryotes. *Trends in*
323 *Ecology & Evolution* 35:43–55.

324 Cavalier-Smith T. 1999. Principles of protein and lipid targeting in secondary symbiogenesis:
325 euglenoid, dinoflagellate, and sporozoan plastid origins and the eukaryote family tree.
326 *Journal of Eukaryotic Microbiology* 46:347–366.

327 Challis R, Richards E, Rajan J, Cochrane G, Blaxter M. 2020. BlobToolKit – Interactive
328 quality assessment of genome assemblies. *G3 (Bethesda)* 10:1361–1374.

329 Criscuolo A, Gribaldo S. 2010. BMGE (Block Mapping and Gathering with Entropy): a new
330 software for selection of phylogenetic informative regions from multiple sequence
331 alignments. *BMC Evolutionary Biology* 10:210.

332 Douglas S, Zauner S, Fraunholz M, Beaton M, Penny S, Deng L-T, Wu X, Reith M,
333 Cavalier-Smith T, Maier U-G. 2001. The highly reduced genome of an enslaved algal
334 nucleus. *Nature* 410:1091–1096.

335 Douglas SE, Murphy CA, Spencer DF, Gray MW. 1991. Cryptomonad algae are evolutionary
336 chimaeras of two phylogenetically distinct unicellular eukaryotes. *Nature* 350:148–
337 151.

338 Gaston D, Susko E, Roger AJ. 2011. A phylogenetic mixture model for the identification of
339 functionally divergent protein residues. *Bioinformatics* 27:2655–2663.

340 Gawryluk RMR, Tikhonenkov DV, Hehenberger E, Husnik F, Mylnikov AP, Keeling PJ.
341 2019. Non-photosynthetic predators are sister to red algae. *Nature* 572:240–243.

342 Greenwold MJ, Merritt K, Richardson TL, Dudycha JL. 2023. A three-genome
343 ultraconserved element phylogeny of cryptophytes. *Protist* 174:125994.

344 Hoef-Emden K, Marin B, Melkonian M. 2002. Nuclear and nucleomorph SSU rDNA
345 phylogeny in the Cryptophyta and the evolution of cryptophyte diversity. *J Mol Evol*
346 55:161–179.

347 Hoff KJ, Stanke M. 2013. WebAUGUSTUS—A web service for training AUGUSTUS and
348 predicting genes in eukaryotes. *Nucleic Acids Research* 41:W123–W128.

349 Iida K, Takishita K, Ohshima K, Inagaki Y. 2007. Assessing the monophyly of chlorophyll-c
350 containing plastids by multi-gene phylogenies under the unlinked model conditions.
351 *Molecular Phylogenetics and Evolution* 45:227–238.

352 Inagaki Y, Blouin C, Susko E, Roger AJ. 2003. Assessing functional divergence in EF-1α
353 and its paralogs in eukaryotes and archaebacteria. *Nucleic Acids Research* 31:4227–
354 4237.

355 Janouškovec J, Horák A, Oborník M, Lukeš J, Keeling PJ. 2010. A common red algal origin
356 of the apicomplexan, dinoflagellate, and heterokont plastids. *Proceedings of the*
357 *National Academy of Sciences* 107:10949–10954.

358 Katoh K, Standley DM. 2013. MAFFT multiple sequence alignment software version 7:
359 improvements in performance and usability. *Mol Biol Evol* 30:772–780.

360 Kim E, Archibald JM. 2013. Ultrastructure and molecular phylogeny of the cryptomonad
361 *Goniomonas avonlea* sp. nov. *Protist* 164:160–182.

362 Kim JI, Moore CE, Archibald JM, Bhattacharya D, Yi G, Yoon HS, Shin W. 2017.
363 Evolutionary dynamics of cryptophyte plastid genomes. *Genome Biology and*
364 *Evolution* 9:1859–1872.

365 Lartillot N, Philippe H. 2004. A Bayesian mixture model for across-site heterogeneities in the
366 amino-acid replacement process. *Molecular Biology and Evolution* 21:1095–1109.

367 Lartillot N, Rodrigue N, Stubbs D, Richer J. 2013. PhyloBayes MPI: Phylogenetic
368 reconstruction with infinite mixtures of profiles in a parallel environment. *Systematic*
369 *Biology* 62:611–615.

370 Lewis LA. 2017. Hold the salt: Freshwater origin of primary plastids. *Proceedings of the*
371 *National Academy of Sciences* 114:9759–9760.

372 Ludwig M, Gibbs SP. 1987. Are the nucleomorphs of cryptomonads and *Chlorarachnion* the
373 vestigial nuclei of eukaryotic endosymbionts? *Annals of the New York Academy of*
374 *Sciences* 503:198–211.

375 Ludwig M, Gibbs SP. 1989. Evidence that the nucleomorphs of *Chlorarachnion reptans*
376 (Chlorarachniophyceae) are vestigial nuclei: Morphology, division and DNA-DAPI
377 fluorescence. *Journal of Phycology* 25:385–394.

Maier U-G, Hofmann CJB, Eschbach S, Wolters J, Igloi GL. 1991. Demonstration of nucleomorph-encoded eukaryotic small subunit ribosomal RNA in cryptomonads. *Molec. Gen. Genet.* 230:155–160.

Manni M, Berkeley MR, Seppey M, Simão FA, Zdobnov EM. 2021. BUSCO update: Novel and streamlined workflows along with broader and deeper phylogenetic coverage for scoring of eukaryotic, prokaryotic, and viral genomes. *Molecular Biology and Evolution* 38:4647–4654.

Martijn J, Vosseberg J, Guy L, Offre P, Ettema TJG. 2018. Deep mitochondrial origin outside the sampled alphaproteobacteria. *Nature* 557:101–105.

Minh BQ, Schmidt HA, Chernomor O, Schrempf D, Woodhams MD, von Haeseler A, Lanfear R. 2020. IQ-TREE 2: New models and efficient methods for phylogenetic inference in the genomic era. *Mol Biol Evol* 37:1530–1534.

Moore CE, Curtis B, Mills T, Tanifuji G, Archibald JM. 2012. Nucleomorph genome sequence of the cryptophyte alga *Chroomonas mesostigmatica* CCMP1168 reveals lineage-specific gene loss and genome complexity. *Genome Biol Evol* 4:1162–1175.

Muñoz-Gómez SA, Hess S, Burger G, Lang BF, Susko E, Slamovits CH, Roger AJ. 2019. An updated phylogeny of the Alphaproteobacteria reveals that the parasitic Rickettsiales and Holosporales have independent origins. *eLife* 8:e42535.

Muñoz-Gómez SA, Mejía-Franco FG, Durnin K, Colp M, Grisdale CJ, Archibald JM, Slamovits CH. 2017. The new red algal subphylum Proteorhodophytina comprises the largest and most divergent plastid genomes known. *Current Biology* 27:1677-1684.e4.

Muñoz-Gómez SA, Susko E, Williamson K, Eme L, Slamovits CH, Moreira D, López-García P, Roger AJ. 2022. Site-and-branch-heterogeneous analyses of an expanded dataset favour mitochondria as sister to known Alphaproteobacteria. *Nat Ecol Evol* 6:253–262.

Park SI, Cho CH, Ciniglia C, Huang T-Y, Liu S-L, Bustamante DE, Calderon MS, Mansilla A, McDermott T, Andersen RA, et al. 2023. Revised classification of the Cyanidiophyceae based on plastid genome data with descriptions of the Cavernulicolales ord. nov. and Galdieriales ord. nov. (Rhodophyta). *Journal of Phycology* 59:444–466.

Petersen J, Ludewig A-K, Michael V, Bunk B, Jarek M, Baurain D, Brinkmann H. 2014. *Chromera velia*, endosymbioses and the Rhodoplex hypothesis—Plastid evolution in cryptophytes, alveolates, stramenopiles, and haptophytes (CASH lineages). *Genome Biology and Evolution* 6:666–684.

Ponce-Toledo RI, Deschamps P, López-García P, Zivanovic Y, Benzerara K, Moreira D. 2017. An early-branching freshwater cyanobacterium at the origin of plastids. *Current Biology* 27:386–391.

Price MN, Dehal PS, Arkin AP. 2010. FastTree 2 – Approximately maximum-likelihood trees for large alignments. *PLOS ONE* 5:e9490.

Prjibelski A, Antipov D, Meleshko D, Lapidus A, Korobeynikov A. 2020. Using SPAdes de novo assembler. *Current Protocols in Bioinformatics* 70:e102.

Pronk LJU, Medema MH. 2022. Whokaryote: Distinguishing eukaryotic and prokaryotic contigs in metagenomes based on gene structure. *Microbial Genomics* 8:000823.

Rambaut A, Drummond AJ, Xie D, Baele G, Suchard MA. 2018. Posterior summarization in bayesian phylogenetics using Tracer 1.7. *Syst Biol* 67:901–904.

Richter DJ, Berney C, Strassert JFH, Poh Y-P, Herman EK, Muñoz-Gómez SA, Wideman JG, Burki F, de Vargas C. 2022. EukProt: A database of genome-scale predicted proteins across the diversity of eukaryotes. *Peer Community Journal* 2:e56.

Robinson JT, Thorvaldsdóttir H, Winckler W, Guttman M, Lander ES, Getz G, Mesirov JP. 2011. Integrative Genomics Viewer. *Nat Biotechnol* 29:24–26.

Sánchez-Baracaldo P, Raven JA, Pisani D, Knoll AH. 2017. Early photosynthetic eukaryotes inhabited low-salinity habitats. *Proc Natl Acad Sci U S A* 114:E7737–E7745.

Sanchez-Puerta MV, Delwiche CF. 2008. A hypothesis for plastid evolution in chromalveolates. *Journal of Phycology* 44:1097–1107.

Sarai C, Tanifuji G, Nakayama T, Kamikawa R, Takahashi K, Yazaki E, Matsuo E, Miyashita H, Ishida K, Iwataki M, et al. 2020. Dinoflagellates with relic endosymbiont nuclei as models for elucidating organellogenesis. *Proceedings of the National Academy of Sciences* 117:5364–5375.

Ševčíková T, Horák A, Klimeš V, Zbránková V, Demir-Hilton E, Sudek S, Jenkins J, Schmutz J, Přibyl P, Fousek J, et al. 2015. Updating algal evolutionary relationships through plastid genome sequencing: did alveolate plastids emerge through endosymbiosis of an ochrophyte? *Sci Rep* 5:10134.

Shimodaira H. 2002. An approximately unbiased test of phylogenetic tree selection. *Syst Biol* 51:492–508.

Smith SA, Dunn CW. 2008. Phyutility: A phyloinformatics tool for trees, alignments and molecular data. *Bioinformatics* 24:715–716.

Steenwyk JL, Buida TJ III, Labella AL, Li Y, Shen X-X, Rokas A. 2021. PhyKIT: A broadly applicable UNIX shell toolkit for processing and analyzing phylogenomic data. *Bioinformatics* 37:2325–2331.

Stiller JW, Schreiber J, Yue J, Guo H, Ding Q, Huang J. 2014. The evolution of photosynthesis in chromist algae through serial endosymbioses. *Nat Commun* 5:5764.

Susko E, Roger AJ. 2007. On reduced amino acid alphabets for phylogenetic inference. *Molecular Biology and Evolution* 24:2139–2150.

Tanifuji G, Onodera NT, Wheeler TJ, Dlutek M, Donaher N, Archibald JM. 2010. Complete nucleomorph genome sequence of the nonphotosynthetic alga *Cryptomonas paramecium* reveals a core nucleomorph gene set. *Genome Biol Evol* 3:44–54.

454 Viklund J, Ettema TJG, Andersson SGE. 2012. Independent genome reduction and
455 phylogenetic reclassification of the oceanic SAR11 clade. *Mol Biol Evol* 29:599–615.

456 Whelan S, Irisarri I, Burki F. 2018. PREQUAL: Detecting non-homologous characters in sets
457 of unaligned homologous sequences. *Bioinformatics* 34:3929–3930.

458 Wong DK, Grisdale CJ, Slat VA, Rader SD, Fast NM. 2023. The evolution of pre-mRNA
459 splicing and its machinery revealed by reduced extremophilic red algae. *Journal of*
460 *Eukaryotic Microbiology* 70:e12927.

461 Yoon HS, Hackett JD, Pinto G, Bhattacharya D. 2002. The single, ancient origin of chromist
462 plastids. *Proceedings of the National Academy of Sciences* 99:15507–15512.

463 Yoon HS, Nelson W, Lindstrom SC, Boo SM, Pueschel C, Qiu H, Bhattacharya D. 2017.
464 Rhodophyta. In: Archibald JM, Simpson AGB, Slamovits CH, editors. Handbook of
465 the Protists. Cham: Springer International Publishing. p. 89–133. Available from:
466 https://doi.org/10.1007/978-3-319-28149-0_33

467

468 **Figure legends**

469 **Figure 1.** Phylogenetic tree placing cryptophyte NMs among Archaeplastida. (**A**) Phylogenetic
470 tree constructed from a concatenation of 180 nucleus/nucleomorph-encoded proteins (51,610
471 positions, 54 taxa) with maximum likelihood (LG+C60+G+F). Branch support values are
472 derived from Bayesian posterior probability (CAT-GTR) and maximum likelihood ultrafast
473 and nonparametric bootstrap. (**B**) Completeness of the individual datasets shown as a schematic
474 representation of the complete supermatrix alignment (gaps in white).

475 **Figure 2.** Results of the tests of topology robustness. (**A–E**) Changes in ultrafast bootstrap
476 support for the sister relationship between cryptophyte NMs and Cyanidiophytina or alternative
477 topologies as calculated based on reduced supermatrices in tests 1–5. (**F**) Principal component
478 analysis of amino acid composition of the individual datasets used in the phylogenetic analyses.
479 (**G**) Simplified schematic representation of the resulting phylogenetic tree with positions of
480 alternative placement of cryptophyte NMs used in test 7 and ultrafast bootstrap support for the
481 sister relationship between cryptophyte NMs and Cyanidiophytina as calculated based on
482 modified supermatrices in tests 6 and 8. (**H**) Results of topology tests calculated with IQ-TREE
483 in test 7.

Figures

Figure 1

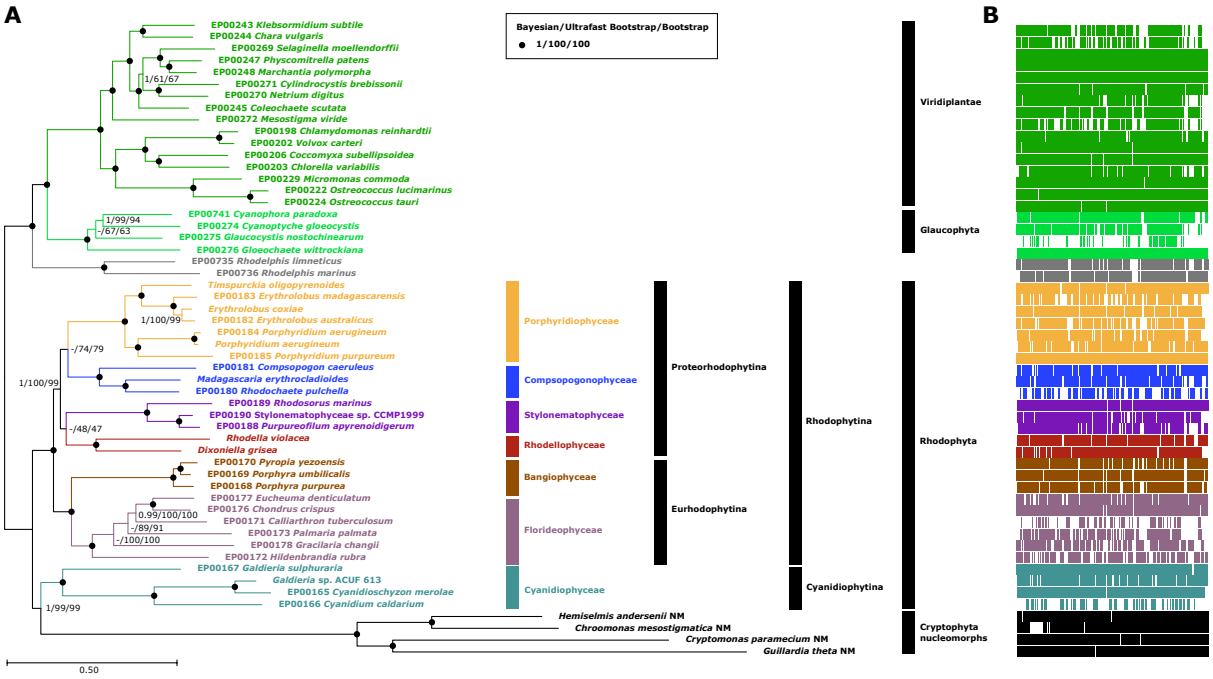

488 **Figure 2**

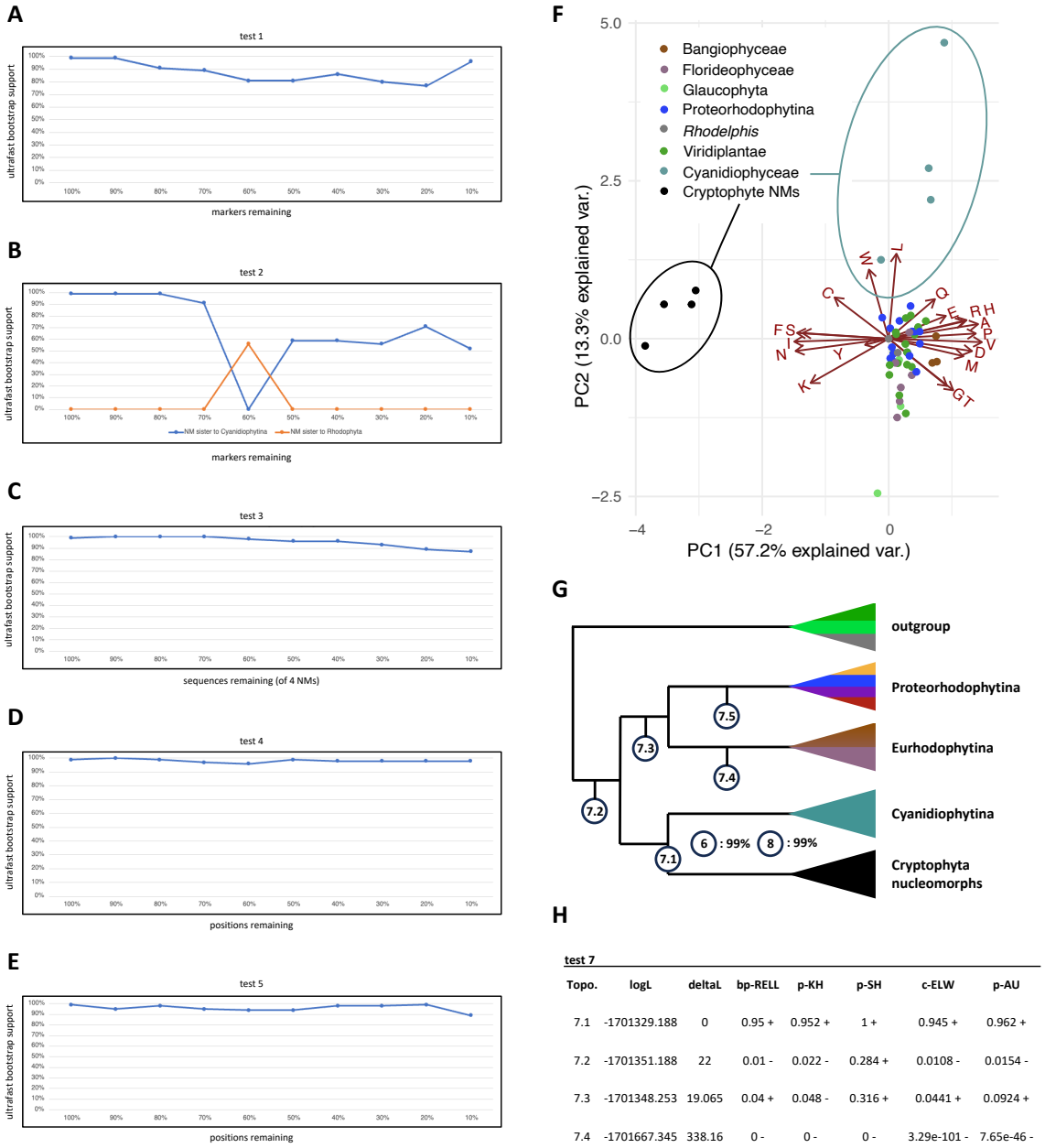

H

test 7

Topo.	logL	deltaL	bp-RELL	p-KH	p-SH	c-ELW	p-AU
7.1	-1701329.188	0	0.95 +	0.952 +	1 +	0.945 +	0.962 +
7.2	-1701351.188	22	0.01 -	0.022 -	0.284 +	0.0108 -	0.0154 -
7.3	-1701348.253	19.065	0.04 +	0.048 -	0.316 +	0.0441 +	0.0924 +
7.4	-1701667.345	338.16	0 -	0 -	0 -	3.29e-101 -	7.65e-46 -
7.5	-1701666.461	337.27	0 -	0 -	0 -	1.98e-99 -	4.11e-52 -

489